THE SLOAN DIGITAL SKY SURVEY REVERBERATION MAPPING PROJECT: SI IV LAG RESULTS FROM TEN YEARS OF DATA

by

Vivian Carvajal

A Thesis Submitted to the Faculty of the

DEPARTMENT OF ASTRONOMY

In Partial Fulfillment of the Requirements

For the Degree of

MASTER OF SCIENCE WITH A MAJOR IN ASTRONOMY AND ASTROPHYSICS

In the Graduate College

THE UNIVERSITY OF ARIZONA

2023

THE UNIVERSITY OF ARIZONA
GRADUATE COLLEGE

As members of the Master's Committee, we certify that we have read the thesis prepared by Vivian Carvajal, titled The Sloan Digital Sky Survey Reverberation Mapping Project: Si IV Lag Results from Ten Years of Data and recommend that it be accepted as fulfilling the thesis requirement for the Master's Degree.

Richard F Green — Date: Apr 26, 2023
Richard F Green

George Rieke — Date: Apr 26, 2023
George Rieke (Apr 26, 2023 15:48 PDT)
George H Rieke

Catherine J Grier — Date: Apr 27, 2023
Catherine J Grier (Apr 27, 2023 11:03 CDT)
Catherine Grier

Marcia J. Rieke — Date: Apr 26, 2023
Marcia J Rieke

Stacey Alberts — Date: Apr 27, 2023
Stacey Alberts (Apr 27, 2023 10:26 PDT)
Stacey Alberts

Final approval and acceptance of this document is contingent upon the candidate's submission of the final copies of the document to the Graduate College.

I hereby certify that I have read this document prepared under my direction and recommend that it be accepted as fulfilling the document requirement.

Richard F Green — Date: Apr 26, 2023
Richard Green
Master's Thesis Committee Chair
Department of Astronomy and Astrophysics

ACKNOWLEDGMENTS

To my dear advisor, Kate Grier: Thank you for taking a chance on me on as your first graduate student. You saw my potential even when I couldn't, and your endless patience and empathy kept me going when I wanted to stop. To my co-advisor, George Rieke: Thank you for adopting me on the home stretch. Your constant support and motivation helped me finish this thesis, and your advice helped me look past it to the future.

To the Department of Astronomy and Steward Observatory: Thank you for the endless support you've given me over the last three years. To my thesis committee: Thank you all for coming together on short notice and accommodating my sudden change in life plan. Thank you for giving your time to read my thesis and attend my defense. To Maxwell Moe and Joe Hoscheidt: Thank you for introducing me to the best part of being an astronomer. I will always be grateful for the knowledge and support you provided.

To all of the friends I've made here in Tucson: Thank you for your patience and support these last three years, through both school and life. You stood by me through my lows and lifted me to my highs, and I will always be thankful for you.

Thank you to my parents, who have always supported my dreams and moved mountains to help me achieve them. I will forever be grateful for the sacrifices you made so that I could have the opportunities I did.

Thank you to my dear cat, Nyx, who curled up at my side for every online lecture, every late night writing crunch, and every moment in between. Your companionship during this period of my life was more important to me than you will ever know.

And finally, to Matthew Wilkin: I would not be writing this today without you. Your unwavering love and support through this experience created the foundation I needed to build myself up when I was so low. I don't think human language will ever be able to express what you mean to me, so for now I will simply say this: I love you.

LAND ACKNOWLEDGMENT

We respectfully acknowledge the University of Arizona is on the land and territories of Indigenous peoples. Today, Arizona is home to 22 federally recognized tribes, with Tucson being home to the O'odham and the Yaqui. Committed to diversity and inclusion, the University strives to build sustainable relationships with sovereign Native Nations and Indigenous communities through education offerings, partnerships, and community service.

DEDICATION

To the fifth-grade version of myself who was just beginning to dream of being a scientist for black holes. To the tenth-grade version of myself who faced the first of many obstacles along the journey and still resolved to pursue this dream. To the undergraduate version of myself who clung to this dream while drowning, and to the graduate version of myself who wielded this dream to claw her way up from the deepest valleys all the way to the stars.

We did it.

TABLE OF CONTENTS

ABSTRACT

We present reverberation-mapping lags and black-hole mass measurements using the Si IV λ1369 blended broad emission line for a sample of 62 quasars monitored as part of the Sloan Digital Sky Survey Reverberation Mapping Project (SDSS-RM). Our spectroscopic and photometric monitoring span a baseline of 4,000 days. We report significant lag detection between the continuum and Si IV emission line in 6 quasars. We use our lag measurements to calculate black hole masses and measure an updated Si IV radius-luminosity relationship. Our results more than double the sample size of quasars with existing Si IV lag measurements. Furthermore, most of our significant lag measurements are for quasars located at $z > 2$, which significantly expands our distance range for successful reverberation mapping. Our Si IV radius-luminosity relationship also agrees with recently measured C IV radius-luminosity relationships, suggesting that both emission lines can provide reliable reverberation-mapping results.

1. INTRODUCTION

Galactic evolution over cosmic time is closely tied to the evolution of central supermassive black holes (SMBH). However, the specific nature of the relation is unknown and difficult to establish (as is thoroughly discussed in Kormendy & Ho 2013). The mass of the SMBH and/or level of AGN activity have been shown to correlate with several properties of the host galaxy, e.g., bulge mass (Kormendy & Ho 2013), circumnuclear star formation (Diamond-Stanic & Rieke 2012), and galaxy environment (Shirasaki et al. 2020)[1]. Given these correlations, measuring the masses of SMBHs at a range of redshifts should help us understand the nature of galaxy evolution over time.

There are very few galaxies for which we can currently spatially resolve the central region, so determining the SMBH mass using kinematics is not feasible for most black holes. Reverberation mapping (RM), however, is an established tool that has measured BH masses for approximately 200 objects out to $z > 3$ (e.g. Bentz & Katz 2015; Shen et al. 2016; Grier et al. 2017, 2019; Kaspi et al. 2021). RM is discussed thoroughly in Cackett et al. (2021), but the general process is summarized here. Light emitted by the accretion disk near the black hole in an active galactic nucleus (AGN) travels in every direction. Some photons travel directly towards us, while others are absorbed and re-emitted by atoms and molecules in the gas around the black hole before being detected on Earth (Figure 1). As a result, measuring changes in the flux of individual emission lines for an AGN can produce a light curve with the same variability features as the accretion disk's continuum but smoothed and delayed on a timescale associated with the radius of the region containing that emission line. Unobscured (Type I) AGNs have broad emission lines originating close to the central engine, an area called the broad line region (BLR) that can be probed using optical reverberation mapping. By assuming the broadening of emission lines in the BLR is dominated by the Doppler effect (representing Keplerian motion), we can combine the radius of the BLR derived from RM with the width of the emission line to calculate the mass of the black hole using the following equation:

$$M_{\rm BH} = \frac{f R_{\rm BLR} \Delta V^2}{G}, \tag{1}$$

where f is the virial factor, a dimensionless parameter whose value depends on the kinematics, geometry, and orientation of the BLR. It is difficult to measure f for individual AGNs, so use of an average value for f was introduced by Onken et al. (2004). Recent discussions of appropriate average values can be found in Woo et al. (2015); Yu et al. (2020). The value depends on the method used to define ΔV, either FWHM or $\sigma_{line,rms}$. The recent analysis of f by Yu et al. (2020) demonstrates that there are still systemic and random errors associated with the virial factor, errors that are very dependent on the AGN sample and velocity tracer used when fitting for f. These errors are one source of uncertainty in black hole masses determined through RM.

[1] But see Masoura et al. (2021) for cautions.

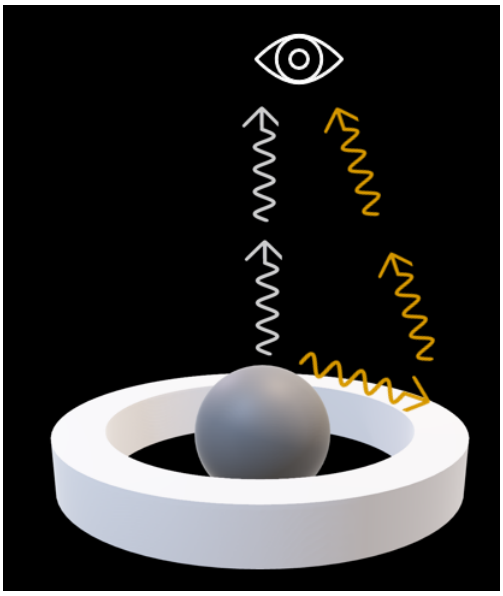

Figure 1. Illustration depicting the reverberation mapping process. The white arrows represent photons travelling directly to the observer, while the orange arrows represent photons being reprocessed by the broad-line region before travelling to the observer.

This paper reports results from the SDSS Reverberation Mapping Project (SDSS-RM), based on extensive spectroscopic data from the Sloan Digital Sky Survey (SDSS). The survey is centered on the Pan-STARRS1 (PS1) medium deep field 07 and also has X-ray coverage from the Chandra X-ray Observatory, making it an interesting field for multi-wavelength studies. The program has monitored 849 broad-line quasars (i.e. very luminous AGNs) within this field for seven years with the goal of increasing the catalog of AGNs with RM-based black-hole mass estimates.

To date, the SDSS-RM program has successfully estimated more than one hundred black hole masses using the Hβ, Mg II, and C IV lines (e.g. Grier et al. 2017, 2019; Homayouni et al. 2020; Shen et al. 2016, 2019). Use of Hβ (4862.63 Å) for RM is well-established (Vestergaard & Peterson 2006), but its long wavelength causes it to shift into the infrared at a redshift of just $z \sim 1$. Since effective reverberation mapping requires consistent and frequent sampling, an observing campaign using existing infrared telescopes (relatively few of which have suitable instrumentation) would be too time-intensive to be prac-

tical. This issue drove researchers to look at ultraviolet emission lines as well. Mg II (2798.75 Å) can also be used for RM, but the masses it produces are not in agreement with those measured with Hβ (Homayouni et al. 2020). C IV (1549.56 Å) has provided some mass estimates at higher redshifts than Hβ, but there are some points of contention regarding how to measure the emission line width since it is prone to broadening caused by winds and outflows (Zuo et al. 2020), although several corrections have been proposed (e.g. Coatman et al. 2017). Finding another emission line that can produce reasonable BH masses will provide a potential check on the accuracy of masses measured with these emission lines and might allow us to use RM to measure black hole masses at higher redshifts, providing another resource for studying galaxy evolution. The importance of adding new lines to such studies is discussed by Homayouni et al. (2020).

This paper presents lag results and black hole mass measurements for quasars observed by the SDSS-RM project using the Si IV emission line (1396.76 Å). In Section 2 we outline the data used in this study. In Section 3 we describe the process used to measure the lags and assess their validity. In Section 4 we discuss our results, along with other applications of our measurements. Finally, in Section 5 we summarize our findings. Throughout this paper, we adopt a ΛCDM cosmology with $\Omega_\Lambda = 0.7$, $\Omega_M = 0.3$, and $h = 0.7$.

2. DATA AND DATA PROCESSING

2.1. *The Quasar Sample*

Our starting sample contained 849 AGNs monitored by the SDSS-RM program in a redshift range of $0.1<z<4.5$. We selected from this sample AGNs with adequate signal to noise ratios (SNRs) and with relatively large variability. From the main sample, 75 AGNs have Si IV light curves with adequate signal to noise (SNR2 > 20)[2]. We then removed sources with significant broad-absorption features (BALs) affecting the Si IV line, reducing our sample to 62 AGNs. This subset of AGNs falls between redshifts 1.68 and 4.33.

2.2. *Spectroscopic Data*

Spectroscopy was performed using the BOSS spectrograph with a cadence of several days during each SDSS observing run. We obtained spectra for a total of 90 epochs distributed over 7 years. The spectra for each object were fit using `PREPSPEC` (Shen et al. 2015, 2016), which provided line widths and calibrated flux measurements for the emission lines (Figure 2). The spectra were also used in conjunction with the SDSS filter bandpasses to create synthetic photometry in the g and i bands.

[2] SNR2 is defined as $\sqrt{\chi^2 - DOF}$, where χ^2 is measured relative to the mean flux of the light curve, and the degrees of freedom DOF is one less than the number of data points in the light curve.

2.3. *Photometric Data*

In addition to the synthetic photometry from the SDSS data, we also acquired supplementary continuum photometry from the Canada France Hawaii Telescope (CFHT), the Zwicky Transient Facility (ZTF), Pan-STARRS1 (PS1), and the Steward Observatory Bok telescope to extend the light curve sampling into bright time for each observing run (Figure 3). We used standard archival data products for the ZTF and PS1 data. The data reduction process for the CFHT and Bok photometry is described in Kinemuchi et al. (2020).

2.4. *Light Curve Inter-Calibration*

For each AGN, the available continuum photometric data from all of the telescopes were merged using the `PyCALI` Python package, whose calibration procedure is described in Li et al. (2014). In all of our light curves, we removed points with errors larger than 3x the median error value of epochs within a single observing season. We also removed points that were more than 3 standard deviations away from the normalized median flux within a single observing season.

3. LAG MEASUREMENTS

To measure the lags for our sample of AGNs, we followed the procedure described by Grier et al. (2019) We first used an interpolated cross-correlation function (ICCF) technique, one of the standard ways to measure lags, implemented by the `PyCCF` Python package (Sun et al. 2018). This method used linear interpolation to fill sampling gaps in the light curves, then measured the cross-correlation function (CCF) between the continuum and emission line light curves. The centroid of the CCF, τ_{cent}, was taken to be the preferred lag. Then we used 5000 Monte Carlo iterations to randomize the flux measurements within their errors and choose a random subset of points to create a posterior distribution of centroids, the peak of which was used to determine the final value of τ_{CCF} and its uncertainty (Figure 4).

We also used the `JAVELIN` (Zu et al. 2011, 2013) modelling package to measure lags. `JAVELIN` used a damped random walk model to fill in sampling gaps in the continuum light curve with MCMC interpolation (Figure 5). Then it smoothed and shifted the interpolated continuum and compared the result to the emission line light curve multiple times in another MCMC run. `JAVELIN` produced a posterior distribution for τ_{JAV}, the best fit lag as determined by the MCMC chain, which we then used to determine the observed lag and errors for the AGN.

We allowed the range of possible lags for `JAVELIN` and `PyCCF` to span between -900 and 900 days in an attempt to recover lags up to 1/3 the length of our baseline of observations.

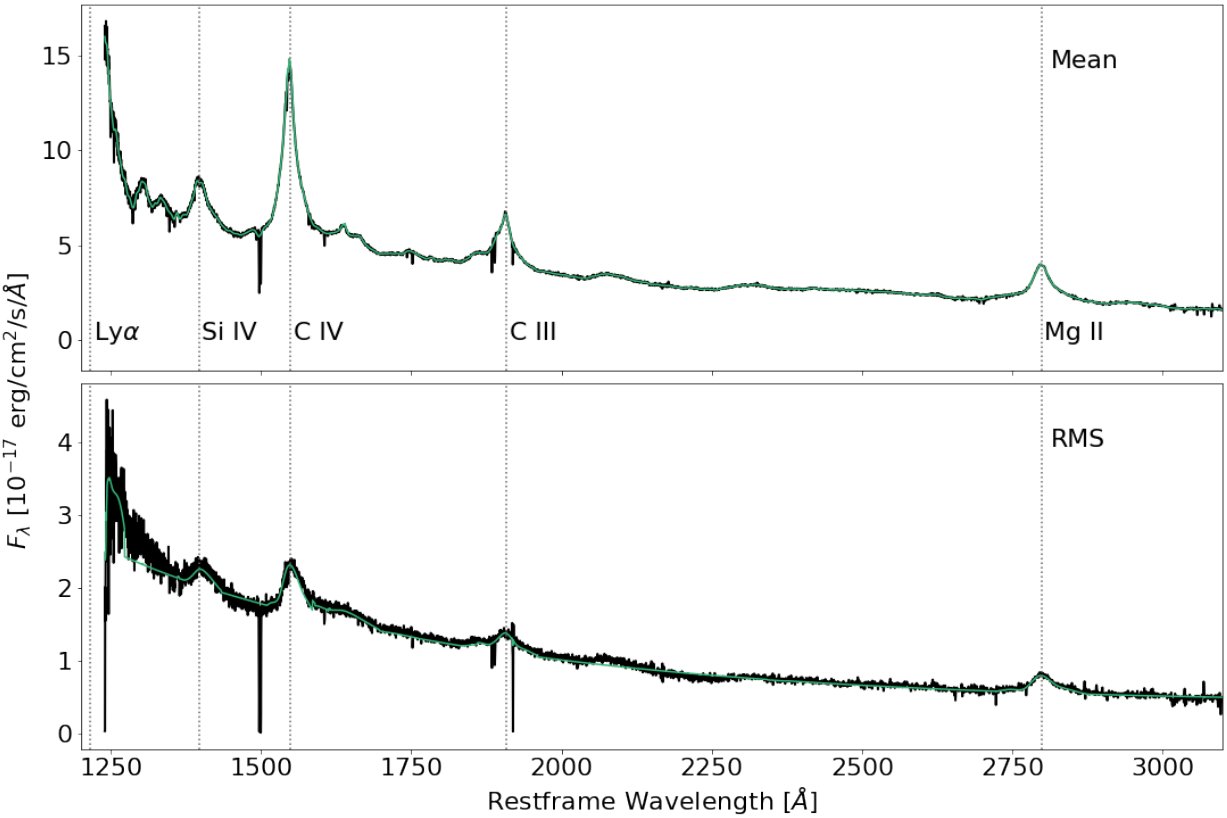

Figure 2. An example of spectral data taken by SDSS. The AGN RM031 was observed multiple times over the course of this campaign, and the mean (top) and rms (bottom) spectra are presented above. The data are shown in black while the `PREPSPEC` models are shown in green. Relevant emission lines are indicated by the grey vertical lines and are labeled at the bottom of the top panel.

3.1. *Alias Identification and Removal*

Since the SDSS light curves have seasonal gaps every six months, `JAVELIN` can heavily sample lags that place the observations in the emission line light curve directly into the seasonal gaps in the continuum light curve, often resulting in a posterior distribution for τ_{JAV} with strong peaks at 180 and 540 days. Since these lag measurements are most likely an artifact rather than something physical, we used a weighting procedure (described by Grier et al. 2019) to suppress these aliases in the posterior distribution (Figure 6). First, we measured the auto-correlation function (ACF) for the continuum. We also used a function $P(\tau)$ that measured what fraction of the continuum and emission light curves overlap at each possible lag. We then convolved the two functions to create a weighting function that downweighted lags with less overlap between the two light curves.

After we applied the weighting scheme to the posterior distribution for τ, we smoothed the distribution with a Gaussian kernel and identified the tallest resulting peak. We used the local minima on each side of the peak to set the lag range used to calculate the final lag. We then defined the best lag τ_{JAV} as the median of the posterior distribution contained within the selected range, and the uncertainties were measured using the 68th percentile of the distribution in the lag range. We also measured the fraction of the posterior distribution excluded from the final lag range, f_{rej}. We performed this alias suppression and lag determination technique on both the τ_{JAV} and τ_{CCF} posterior distributions.

3.2. *Lag Significance Tests*

After we measured our lags and errors, we set three criteria for defining a significant lag:

1. The measured lag must be positive, since there is no physical reason that the continuum emission should trail the BLR emission.

2. The measured lag should not be consistent with a lag of zero days, with 1σ significance.

3. When using `JAVELIN` , f_{rej} must be less than 0.4. In other words, 60% of the posterior distribution must fall within the range of possible lags we select. If f_{rej} is larger, this might mean that `JAVELIN` was unable to clearly determine the best observational lag and continued to sample the entire parameter space.

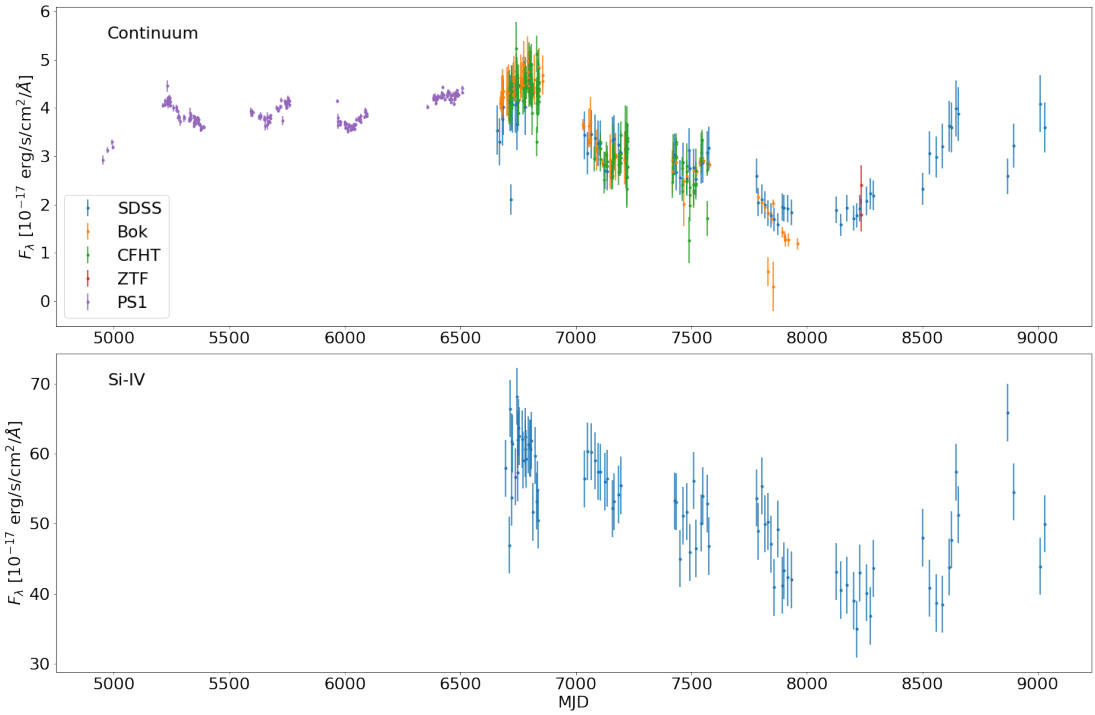

Figure 3. The processed continuum and Si IV light curves for RM031. Continuum photometry from all of the telescopes was merged using `PyCALI`, then points more than 3 standard deviations away from the median flux and points with errors larger than 3 times the median error value of observations were removed from each observing season. Note that the SDSS points in the continuum light curve are synthetic photometry calculated using spectra and filter bandpasses, while the points for the Si IV light curve are simply an integrated flux at the position of the emission line in the spectrum.

Applying these criteria left us with 24 AGN with significant lags from our original sample (Figure 7).

For each AGN that passed these criteria, we compared τ_{JAV} to τ_{CCF} to check for internal consistency (Table 1, Figure 8). We rejected AGNs that did not have agreement between the two lags within 1σ. We also noted that the potential for disagreement among different methods increases for lags longer than about 450 days (e.g. Grier et al. 2019). With this caveat in mind, we manually reviewed the light curves and lag distributions for AGNs with measured lags longer than 450 days. We concluded that the results were reasonable for all of these AGNs and elected to keep them in the sample for further analysis, subject to additional tests of validity.

There were three AGNs with posterior lag distributions heavily sampled at the upper boundary of the parameter space and with internal consistency between τ_{JAV} and τ_{CCF}. For these three AGNs, we re-ran `JAVELIN` while extending the upper lag range to 1400 days to check if the measured lag was an artifact or reasonable. Two of the objects, RM430 and RM780, produced a lag consistent with their original measured lag. The lag for the third AGN, RM207, shifted significantly longer than the original lag, following the edge of the parameter space. Combining these results with the quality of the light curves for these objects leads us to more strongly trust the lag result for RM430 and RM780, but be skeptical of the results for RM207, although we will still report the final results of our analysis.

3.3. *False Positive Rate*

To further test the 19 AGNs with lags that passed our criteria, we performed a simulation technique as described in Homayouni et al. (2020). For each AGN, we paired the continuum light curve with 50 Si IV light curves randomly selected from the rest of the starting sample and performed our `JAVELIN` analysis with each pair. Any lag that passed our initial significance criteria would be a false positive since the two light curves were not physically correlated, so we defined the false positive rate (FPR) for each AGN as the fraction of the measured lags that passed our criteria. This technique provided a conservative estimate of the likelihood of measuring a lag when one isn't actually present. We chose to eliminate AGNs with an FPR larger than 0.25. This filtered our number of significant lags down to six (Figure 9).

4. DISCUSSION

4.1. *The Si IV Blend*

The Si IV emission line at 1396.76 Å is actually a blend consisting of multiple lines both from Si IV and O IV]

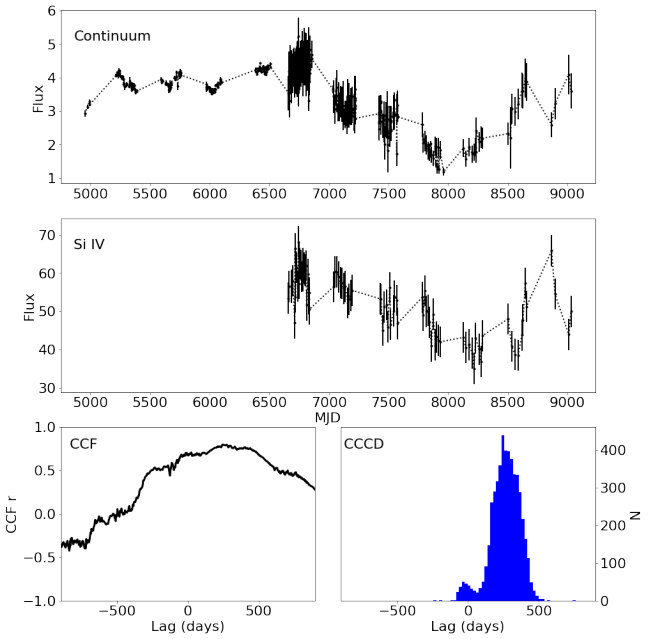

Figure 4. Result from a `PyCCF` run on the light curves from RM031, where the sampling gaps are filled using a linear interpolation (top two panels). `PyCCF` adjusts the observed fluxes within their errors through 5000 Monte Carlo iterations. The cross-correlation function (CCF) for a single iteration is shown on the lower left, and the final centroid distribution (CCCD) is shown on the lower right. This distribution was used to calculate the final CCF lag τ_{CCF} and its uncertainty.

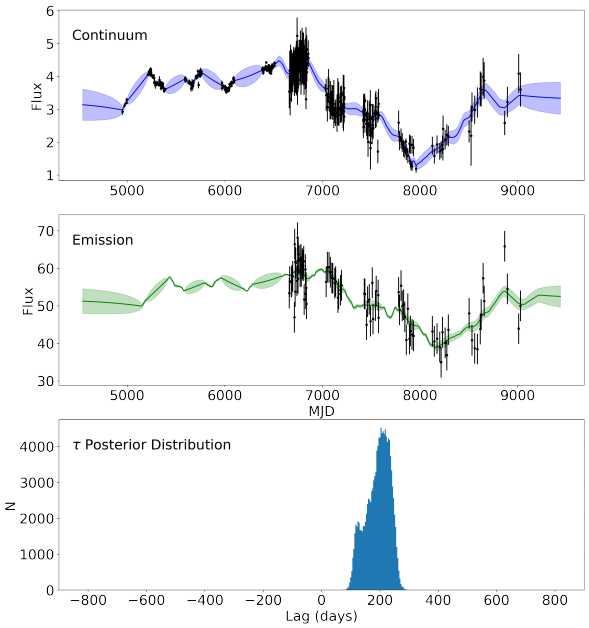

Figure 5. Result from running `JAVELIN` on the light curves from RM031. The top two panels show `JAVELIN` 's damped random walk model of the continuum light curve, along with a smoothed, shifted, and scaled version of the model imposed on the Si IV light curve. `JAVELIN` adjusts the model parameters to best fit both light curves through an MCMC process. The bottom panel shows the posterior distribution for τ, the shift parameter, which we analyzed to determine the final `JAVELIN` lag τ_{JAV} and its uncertainty.

emission. The resolution of the SDSS spectra is not fine enough to resolve the individual lines for the targets in our sample, and the broadening associated with the AGN would probably make this impossible, so the line flux for our light curves is technically the flux for the entire complex.

A comparison of the Si IV complex FWHM with both C IV and Mg II line widths (Table 2) shows that overall the line widths for the complex are comparable to those of the cleaner emission lines. Assuming that the main source of broadening is the Doppler effect due to gas kinematics, it is therefore reasonable to assume that the Si IV complex is moving similarly to the other emission lines within the BLR. This result suggests that we might be able to use the FWHM of the Si IV feature to estimate the AGN BH mass, albeit with moderate error. A study of a larger sample of AGNs (Table 3) reveals that the average ratio of the C IV line width to the Si IV line width is 0.926 while the median ratio is 0.87. Since C IV emission lines are already modestly broadened by outflows (Coatman et al. 2019, Dalla Bontà et al. 2020), caution should be taken for wider use of Si IV in this fashion. However, since Si IV broadening may be dominated by multiple line components rather than winds and outflows, it may be possible to correct for the extra components in the future, making the Si IV emission line more reliable for BH mass determination.

4.2. *Si* IV *Radius-Luminosity Relation*

Previously, Lira et al. (2018) determined the Si IV radius-luminosity (R-L) relation to be

$$\frac{R_{\rm Si\,IV}}{10\ \text{lt-days}} = (0.10 \pm 0.10) \left[\frac{\lambda L_\lambda(1350\text{Å})}{10^{43}\text{erg s}^{-1}}\right]^{0.58\pm0.16} \quad (2)$$

using three AGNs from their own study and two AGNs from previous studies.

Here, we present an updated estimate for the Si IV radius-luminosity relation with the addition of our six AGNs, all falling within the previous luminosity gap. A linear regression was conducted using the BCES method (Akritas & Bershady 1996), taking the mean of the positive and negative lag error as the uncertainty and using the `BCES` Python module (Nemmen 2021). The equation resulting from our fit is

$$\frac{R_{\rm Si\,IV}}{10\ \text{lt-days}} = (0.22 \pm 0.14) \left[\frac{\lambda L_\lambda(1350\text{Å})}{10^{43}\text{erg s}^{-1}}\right]^{0.53\pm0.11} \quad (3)$$

This equation is very close to the equation determined by Lira et al. (2018).

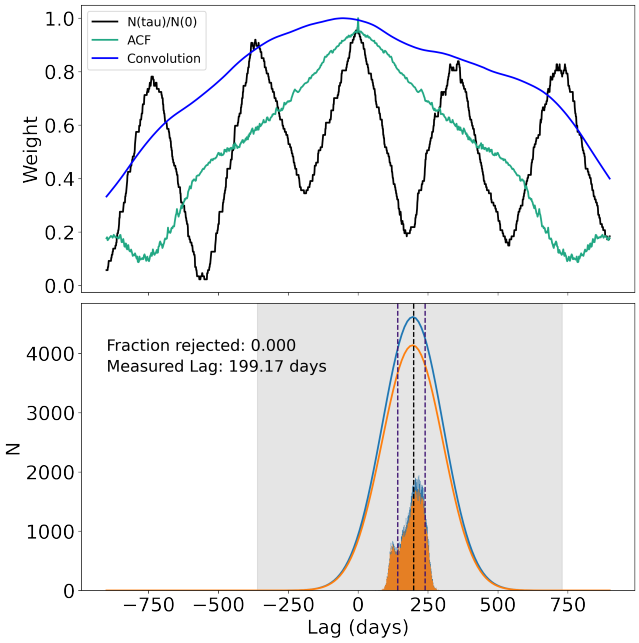

Figure 6. The alias downweighting procedure applied to the posterior distribution of τ. The top panel illustrates the development of a weighting scheme that prioritizes lags that maximize overlap between the two light curves. We then applied the weights to the posterior distribution as shown in the bottom panel, where the blue histogram and Gaussian fit are the original distribution and the orange histogram and fit are the final distribution. We then took the median of the distribution contained within the tallest peak of the Gaussian fit (the shaded area) to be τ_{jav} and calculated uncertainties (indicated by the dashed black and purple lines, respectively). We also noted the fraction of the posterior distribution not contained within the peak, f_{rej}.

A recent study by Kaspi et al. (2021) measured the C IV R-L relation to be

$$\frac{R_{\rm C\,IV}}{10\ \text{lt-days}} = (0.34 \pm 0.11) \left[\frac{\lambda L_\lambda(1350\text{Å})}{10^{43}\text{erg s}^{-1}}\right]^{0.45\pm0.05} \quad (4)$$

using the BCES method. We find that this C IV R-L relation is consistent with our Si IV R-L relation within one sigma (Figure 10). Furthermore, both lines have a slope close to a square-root of theluminosity curve, the expected value based on the assumption that the level of irradiation has a dominant role in the structure of the line-emitting region (e.g. Bentz et al. 2013).

Peterson (1993) showed that the reverberation reaction times for high ionization lines such as C IV are shorter than those for Hβ. This behavior led to the development of models invoking ionization stratification (Baldwin et al. 1995), i.e., that for a given line there is a narrow range of distance from the exciting source and of density that is optimum for reprocessing efficiency, and

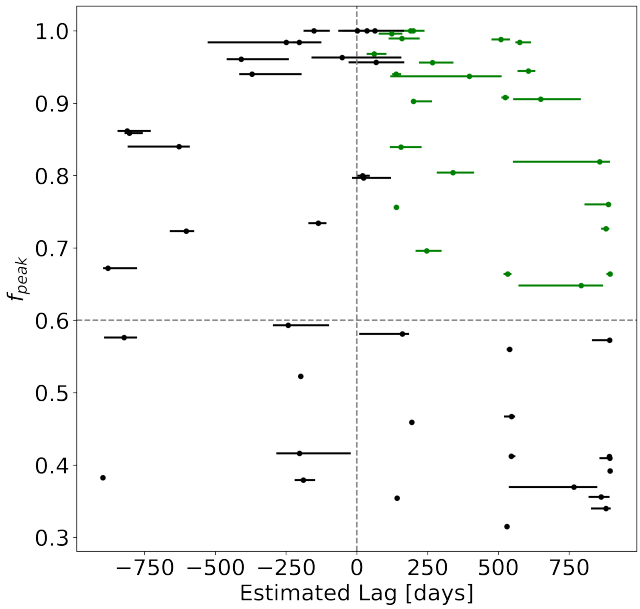

Figure 7. Selecting candidates for significant lag detections from the `JAVELIN` results. Green points indicate AGNs with lags inconsistent with zero and with more than 60% of the posterior distribution for τ contained within the peak.

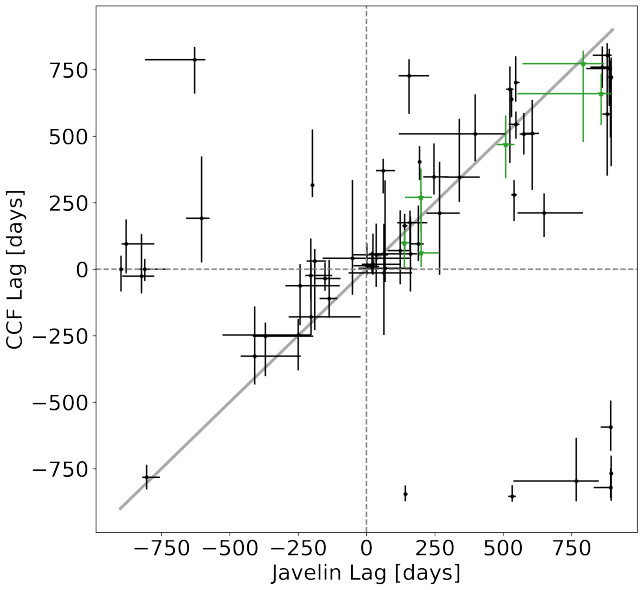

Figure 8. Comparison of `JAVELIN` lag results to `PyCCF` lag results for our full sample. AGNs that passed our initial significance criteria (those located in the top right quadrant) were checked for agreement between τ_{JAV} and τ_{CCF} before running our simulation technique. The green points are our final sample of AGNs that pass all of our significance criteria.

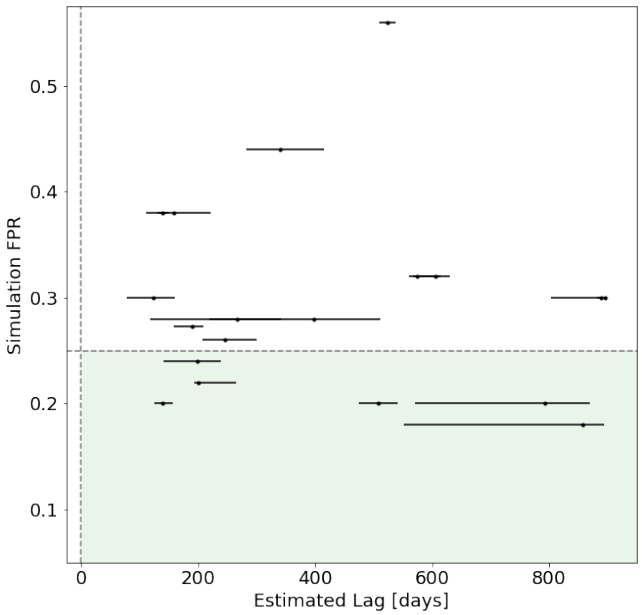

Figure 9. Further selection of AGNs with significant lags through simulated false-positive rates (FPRs). Each AGN's continuum light curve was randomly paired with fifty Si IV light curves and analyzed as done originally. The simulation FPR for each AGN was defined as the fraction of these pairs that would qualify as significant based on our original criteria. We set an FPR of 0.25 as our upper limit, and the AGNs that passed are located in the lower region on the plot.

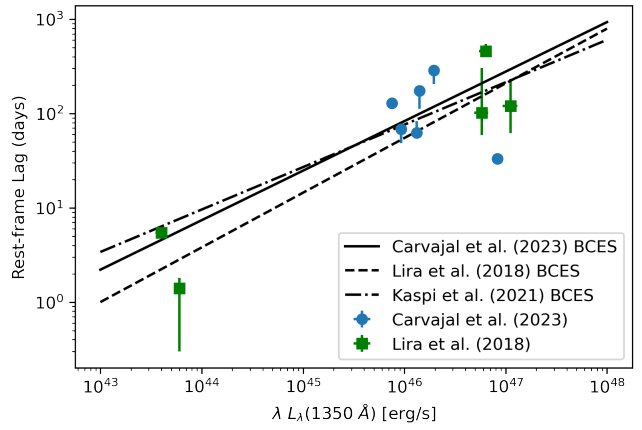

Figure 10. Radius-luminosity relation for Si IV . The blue circles are the high-quality cases from this work, while the green squares are the AGNs used to derive the R-L relation in Lira et al. (2018) (later corrected by Lira et al. (2020)). The line measured by Kaspi et al. (2021) is for C IV , whose R-L relation is expected to agree with that of Si IV .

Table 1. SDSS-RM Observed Lag Detections

RMID*	z	τ_{JAV} (days)	τ_{CCF} (days)	Rating[a]
010	3.230	$156.0^{+73.2}_{-39.0}$	$726.7^{+62.3}_{-142.6}$	Rejected
031	1.909	$199.2^{+40.3}_{-57.7}$	$269.4^{+108.9}_{-130.2}$	Confirmed
180	3.111	$649.4^{+142.3}_{-97.3}$	$211.4^{+73.5}_{-90.9}$	Rejected
190	1.993	$575.2^{+40.0}_{-14.8}$	$507.3^{+79.5}_{-76.7}$	Provisional
207	2.619	$880.2^{+11.5}_{-17.3}$	$582.4^{+145.8}_{-231.3}$	Rejected
237	2.394	$139.3^{+10.7}_{-8.6}$	$163.4^{+44.0}_{-91.0}$	Confirmed
251	2.204	$339.4^{+75.4}_{-56.5}$	$346.0^{+219.1}_{-94.1}$	Confirmed
282	3.363	$246.5^{+53.5}_{-38.9}$	$347.0^{+125.6}_{-66.6}$	Confirmed
342	1.699	$606.2^{+24.6}_{-38.2}$	$509.8^{+125.9}_{-212.0}$	Provisional
430	3.906	$857.9^{+37.0}_{-306.3}$	$660.0^{+73.6}_{-118.5}$	Provisional
451	2.678	$190.1^{+19.4}_{-32.2}$	$94.7^{+144.4}_{-64.4}$	Confirmed
508	3.207	$139.0^{+17.6}_{-13.5}$	$98.4^{+49.0}_{-91.3}$	Confirmed
555	2.164	$532.7^{+13.8}_{-13.8}$	$-854.0^{+41.4}_{-20.5}$	Rejected
562	2.773	$61.1^{+43.7}_{-26.6}$	$370.0^{+45.2}_{-85.7}$	Rejected
591	2.103	$266.9^{+74.3}_{-47.2}$	$210.5^{+193.1}_{-231.4}$	Confirmed
609	2.215	$200.3^{+65.3}_{-7.4}$	$60.9^{+231.6}_{-53.4}$	Confirmed
611	1.866	$888.4^{+10.2}_{-84.3}$	$754.0^{+74.3}_{-141.0}$	Provisional
613	2.350	$524.1^{+13.7}_{-13.7}$	$676.1^{+86.2}_{-276.7}$	Provisional
616	2.316	$895.1^{+4.5}_{-13.4}$	$722.2^{+72.6}_{-335.5}$	Rejected
623	2.957	$508.9^{+32.5}_{-33.3}$	$468.6^{+108.7}_{-127.0}$	Provisional
624	2.085	$397.7^{+113.6}_{-279.7}$	$508.8^{+148.1}_{-103.3}$	Provisional
671	1.982	$159.1^{+63.2}_{-47.0}$	$174.8^{+45.6}_{-104.0}$	Confirmed
765	2.977	$123.7^{+36.8}_{-46.1}$	$69.9^{+151.3}_{-127.2}$	Confirmed
780	1.772	$792.7^{+77.5}_{-221.9}$	$772.9^{+48.7}_{-295.1}$	Provisional

*The AGNs listed in bold font are the final sample that passed all of our criteria.

[a]In this table, the Rating is defined as the following:
Rejected: There is not internal consistency between τ_{JAV} and τ_{CCF}.
Provisional: There is internal consistency between τ_{JAV} and τ_{CCF}. Lags are longer than 450 days but an additional review of the data resulted in accepting this source.
Confirmed: There is internal consistency between τ_{JAV} and τ_{CCF}, and both of the lags are shorter than 450 days.

which will dominate the emission by that line. With sufficiently intense reverberation monitoring, this behavior can be used to map the ionization structure of the BLR (Williams et al. 2020; Horne et al. 2021). The ionization energies of C IV and Si IV are comparable, and the consistency of the C IV R-L relation with the Si IV R-L one suggests that they come from similar regions in the BLR.

Table 2. Confirmed Sample Spectral Line Widths (km s^{-1})

RMID	SiIV	CIV	MgII
	FWHM	FWHM	FWHM
031	5504.0 ± 68.0	4674.2 ± 426.7	3727.0 ± 17.0
237	5725.0 ± 59.0	5212.7 ± 19.3	4921.0 ± 40.0
251	4947.0 ± 231.0	3801.0 ± 84.0	1440.0 ± 66.0
282	3278.0 ± 554.0	3769.0 ± 46.0	···
451	8721.0 ± 276.0	6242.1 ± 26.6	6004.0 ± 936.0
508	1816.0 ± 34.5	3177.9 ± 851.0	···
591	4990.0 ± 59.0	9081.0 ± 699.0	6972.0 ± 64.0
609	3828.0 ± 19.0	3706.4 ± 12.5	3425.0 ± 16.0
671	5154.0 ± 84.0	4147.6 ± 18.6	4061.0 ± 29.0
765	4209.0 ± 46.0	2919.6 ± 20.4	···

4.3. *Black Hole Mass Estimates*

To measure the mass of each AGN SMBH, we use Equation 1, with $\sigma_{Si\,IV,rms}$ as measured by `PREPSPEC`, for ΔV and the `JAVELIN` rest-frame lag for R_{BLR}. Since we use $\sigma_{Si\,IV,rms}$, we adopt a value of 4.47 ± 1.23 for f (Woo et al. 2015). The final BH masses are shown in Table 4. The uncertainties for the masses were calculated using standard error propagation with the uncertainties in f, $\sigma_{Si\,IV,rms}$, and the rest lag. The masses range from 10^7 to 10^9 $M_\odot$. A literature search found no previous RM masses for any of the AGNs with accepted results from our sample, so we are unable to compare our results to those of other emission lines. As mentioned before, the Si IV and C IV emission lines behave similarly with respect to line width changes and ionization energy. Therefore, we expect the quality of the Si IV BH masses to be similar to the quality of previously measured C IV BH masses.

Previous papers have indicated several sources of large systematic uncertainty when measuring black hole masses. Krolik (2001) noted that our lack of information about the exact causes of dynamics in the BLR, along with inclination effects, could result in systematic errors in mass measurements of a factor of at least 3. Peterson et al. (2004) found that the systematic uncertainty is typically slightly smaller than a factor of 3, with a main contributor being narrow-line contamination in the broad-line spectrum. However, they noted that $\sigma_{\rm line}$ as line width is less affected by this issue than FWHM. Collin et al. (2006) found a similar result for $\sigma_{\rm line}$, and they used this result to also determine a statistical value for $\langle f \rangle$. To attempt to account for this systematic uncertainty, we add 0.16 dex in quadrature to the statistical uncertainty in the virial product, a number determined from repeated mass measurements of NGC 5548 (Fausnaugh et al. 2017).

Table 3. Grier et al. (2019) Gold Sample Observed Spectral Line Widths (km s^{-1})

RMID	SiIV	CIV	MgII
	FWHM	FWHM	FWHM
032	2029.0 ± 145.0	2369.0 ± 16.9	2242.0 ± 34.0
036	4946.0 ± 66.0	5075.5 ± 16.0	4764.0 ± 26.0
052[b]	3453.0 ± 37.0	3217.0 ± 10.3	1985.0 ± 17.0
057	3605.0 ± 54.0	2883.4 ± 6.9	2379.0 ± 20.0
058	4020.0 ± 150.0	3672.2 ± 16.9	4822.0 ± 102.0
064[b]	1378.0 ± 57.0	4326.1 ± 22.6	2232.0 ± 37.0
128[b]	8525.0 ± 1385.0	4914.0 ± 123.0	6131.0 ± 405.0
130	4090.0 ± 118.0	3504.4 ± 18.0	2883.0 ± 55.0
144	4010.0 ± 107.0	5352.7 ± 22.7	3484.0 ± 45.0
145	4945.0 ± 354.0	4704.0 ± 80.0	5322.0 ± 73.0
161	3655.0 ± 856.0	2724.5 ± 19.7	3510.0 ± 107.0
181	3358.0 ± 1546.0	2558.0 ± 29.0	4573.0 ± 113.0
201	5612.0 ± 82.0	5657.0 ± 21.0	3705.0 ± 71.0
231	6388.0 ± 409.0	6250.0 ± 55.0	5034.7 ± 20.4
237	5725.0 ± 59.0	5212.7 ± 19.3	4921.0 ± 40.0
245	7102.0 ± 4811.0	6886.0 ± 59.0	9112.0 ± 89.0
249	3454.0 ± 164.0	1849.6 ± 8.9	2091.0 ± 50.0
256	4794.0 ± 362.0	2985.0 ± 34.0	4708.0 ± 95.0
266[ab]	3610.0 ± 1666.0	4657.9 ± 21.9	3718.0 ± 535.0
269	3130.0 ± 172.0	2846.0 ± 27.0	1643.0 ± 88.0
295	4841.0 ± 119.0	4272.6 ± 29.8	3569.0 ± 78.0
298	4201.0 ± 131.0	3141.3 ± 21.1	3157.0 ± 28.0
312	7061.0 ± 973.0	7091.0 ± 76.0	7570.0 ± 97.0
332	3794.0 ± 78.0	1868.7 ± 8.4	1859.0 ± 607.0
346	831.0 ± 1341.0	3414.4 ± 68.1	4632.0 ± 60.0
362[b]	6626.0 ± 654.0	5931.0 ± 43.0	6721.0 ± 81.0
386	4785.0 ± 117.0	3078.1 ± 29.7	3055.0 ± 61.0
387	5724.0 ± 59.0	4014.6 ± 16.4	4167.0 ± 55.0
389	9048.0 ± 280.0	4694.9 ± 23.6	5943.0 ± 81.0
401	4829.0 ± 124.0	3488.0 ± 19.5	3868.0 ± 41.0
408[b]	4846.0 ± 830.0	4253.5 ± 17.1	4664.0 ± 42.0
411	4984.0 ± 371.0	3884.0 ± 35.0	2861.0 ± 71.0
470	7761.0 ± 442.0	3653.0 ± 28.0	3425.0 ± 81.0
485	8656.0 ± 141.0	6741.3 ± 26.6	8386.0 ± 1843.0
496	3968.0 ± 78.0	2127.1 ± 13.3	2601.0 ± 79.0
499	4932.0 ± 656.0	2461.0 ± 31.0	2954.0 ± 359.0
506[b]	6141.0 ± 1692.0	3984.1 ± 16.0	7514.0 ± 85.0
527	4065.0 ± 3409.0	6945.0 ± 274.0	6885.0 ± 89.0
549	3965.0 ± 124.0	4256.0 ± 30.0	2964.0 ± 46.0
554	4330.0 ± 114.0	3789.4 ± 23.1	3544.0 ± 34.0
562[a]	6049.2 ± 21.8	5781.5 ± 21.5	···
686	5465.0 ± 122.0	3898.4 ± 21.3	3470.0 ± 38.0
689	4752.0 ± 159.0	2863.4 ± 15.9	3165.0 ± 51.0
722[ab]	4433.0 ± 51.0	6587.0 ± 45.0	4460.0 ± 117.0
734	5446.0 ± 187.0	5787.0 ± 92.0	6554.0 ± 93.0
809[b]	5516.0 ± 1317.0	11256.0 ± 100.0	6940.0 ± 174.0
827	3362.0 ± 420.0	2942.1 ± 18.6	3706.0 ± 108.0

[a] These AGNs have significant BAL features in SiIV.

[b] These AGNs have significant BAL features in CIV.

Single-epoch BH mass estimations are critical for studying the evolution of SMBHs back to their formation in the early universe since the measurements require fewer telescope resources. Reverberation mapping therefore is an essential tool since it can calibrate the relationships used to make single-epoch mass estimates. Despite the multiple sources of uncertainty in our Si IV mass estimates (e.g. the blending, systematic uncertainties), the consistency in behavior between Si IV with C IV , an established emission line to use in reverberation mapping studies, increases our confidence in this calibration. Once Si IV is further calibrated to correct for blending with O IV] , the emission line will be very helpful as a single-epoch indicator at higher redshifts.

5. SUMMARY

With seven years of spectroscopic data from the SDSS-RM program, along with supplementary photometric data from multiple other telescopes, we searched for time delays between the continuum and the Si IV emission-line in 62 quasars.

1. We defined securely detected lags as cases where the ICCF and `JAVELIN` lags were consistent with each other and both lags were shorter than 450 days. We defined insecure lags as cases with internal consistency between lag measurements but where one or both lags were longer than 450 days. After further vetting for quality, we accepted most of these latter lags for further analysis. We defined our final sample of significant lags as secure or insecure lags with a simulation FPR less than 0.25.

2. We found six AGNs with significant lags. The AGNs span a redshift range of $1.77 < z < 3.91$.

3. We calculated BH masses for these six AGNs using rest-frame lags and $\sigma_{\mathrm{Si\,IV,rms}}$.

4. We fit a new radius-luminosity relation for Si IV that improves upon an existing relation measured by Lira et al. (2018). This R-L relation for Si IV agrees well with a recently measured R-L relation for C IV (Kaspi et al. 2021), as might be expected from their similar ionization energies. This consistency, along with the closeness of the slopes of both relations to the expected square-root behavior (Bentz et al. 2013), supports the validity of RM with these lines to determine black hole properties.

In conclusion, for AGNs with a strong enough Si IV signal, this emission line looks promising for measuring significant lag detections. However, the blended nature of the line with O IV] means that single-epoch spectroscopic line widths cannot be assumed to only be a result of velocity dispersion and therefore may not provide accurate BH mass estimates without an additional calibration effort. Nevertheless, since Si IV is capable of measuring significant lags, we can combine Si IV lags with lags from other emission lines, when possible, to study the stratification of ions in the BLR. Additionally, two AGNs in our sample are located at $z > 3$, demonstrating the efficacy of Si IV as a probe for more distant AGNs. These applications will be enhanced as additional measurements are obtained under the SDSS-V Black Hole Mapper (BHM) survey.

VC and CJG acknowledge support from NSF grants AST-2009949 and AST-2108667. The work of VC and GHR was also supported by grant 80NSSC18K0555, and contract NAS5-02105, both from NASA Goddard Space Flight Center to the University of Arizona.

This work is based on observations obtained with MegaPrime/MegaCam, a joint project of CFHT and CEA/DAPNIA, at the Canada-France-Hawaii Telescope (CFHT) which is operated by the National Research Council (NRC) of Canada, the Institut National des Sciences de l'Univers of the Centre National de la Recherche Scientifique of France, and the University of Hawaii. The authors recognize the cultural importance of the summit of Maunakea to a broad cross section of the Native Hawaiian community. The astronomical community is most fortunate to have the opportunity to conduct observations from this mountain.

Funding for the Sloan Digital Sky Survey IV has been provided by the Alfred P. Sloan Foundation, the U.S. Department of Energy Office of Science, and the Participating Institutions. SDSS-IV acknowledges support and resources from the Center for High-Performance Computing at the University of Utah. The SDSS web site is www.sdss.org.

SDSS-IV is managed by the Astrophysical Research Consortium for the Participating Institutions of the SDSS Collaboration including the Brazilian Participation Group, the Carnegie Institution for Science, Carnegie Mellon University, the Chilean Participation Group, the French Participation Group, Harvard-Smithsonian Center for Astrophysics, Instituto de Astrofísica de Canarias, The Johns Hopkins University, Kavli Institute for the Physics and Mathematics of the Universe (IPMU) / University of Tokyo, the Korean Participation Group, Lawrence Berkeley National Laboratory, Leibniz Institut für Astrophysik Potsdam (AIP), Max-Planck-Institut für Astronomie (MPIA Heidelberg), Max-Planck-Institut für Astrophysik (MPA Garching), Max-Planck-Institut für Extraterrestrische Physik (MPE), National Astronomical Observatories of China, New Mexico State University, New York University, University of Notre Dame, Observatário Nacional / MCTI, The Ohio State University, Pennsylvania State University, Shanghai Astronomical Observatory, United Kingdom Participation Group, Universidad Nacional Autónoma de México, University of Arizona, University of Colorado Boulder, University of Oxford, University of Portsmouth, University of Utah, University of Virginia,

Table 4. Line Widths, Virial Products, and Black Hole Mass Estimates

RMID	z	Rest Lag (days)	FWHM (km s^{-1})	$\sigma_{\rm rms}$ (km s^{-1})	VP $10^7 M_\odot$	M_{BH} $10^7 M_\odot$
031	1.909	$68.5^{+13.9}_{-19.8}$	5504 ± 68	2504 ± 19	$8.4^{+2.2}_{-2.8}$	$37.5^{+14.2}_{-16.1}$
430	3.906	$174.9^{+7.5}_{-62.4}$	6080 ± 181	2058 ± 12	$14.5^{+2.4}_{-5.7}$	$64.6^{+20.8}_{-31.0}$
508	3.207	$33.0^{+4.2}_{-3.2}$	1816 ± 34	987 ± 7	$0.6^{+0.1}_{-0.1}$	$2.8^{+1.0}_{-0.9}$
609	2.215	$62.3^{+20.3}_{-2.3}$	3828 ± 19	2714 ± 18	$9.0^{+3.3}_{-1.5}$	$40.0^{+18.3}_{-12.9}$
623	2.957	$128.6^{+8.2}_{-8.4}$	4163 ± 57	1708 ± 10	$7.3^{+1.3}_{-1.3}$	$32.7^{+10.7}_{-10.7}$
780	1.772	$286.0^{+28.0}_{-80.0}$	4347 ± 37	2245 ± 23	$28.1^{+5.3}_{-9.1}$	$125.7^{+42.0}_{-53.4}$

University of Washington, University of Wisconsin, Vanderbilt University, and Yale University.

We thank the Bok and CFHT Canadian, Chinese, and French TACs for their support. This research uses data obtained through the Telescope Access Program (TAP), which is funded by the National Astronomical Observatories, Chinese Academy of Sciences, and the Special Fund for Astronomy from the Ministry of Finance in China.

REFERENCES

Akritas, M. G., & Bershady, M. A. 1996, ApJ, 470, 706, doi: 10.1086/177901

Baldwin, J., Ferland, G., Korista, K., & Verner, D. 1995, ApJL, 455, L119, doi: 10.1086/309827

Bentz, M. C., & Katz, S. 2015, PASP, 127, 67, doi: 10.1086/679601

Bentz, M. C., Denney, K. D., Grier, C. J., et al. 2013, ApJ, 767, 149, doi: 10.1088/0004-637X/767/2/149

Cackett, E. M., Bentz, M. C., & Kara, E. 2021, iScience, 24, 102557, doi: 10.1016/j.isci.2021.102557

Coatman, L., Hewett, P. C., Banerji, M., et al. 2017, MNRAS, 465, 2120, doi: 10.1093/mnras/stw2797

Coatman, L., Hewett, P. C., Banerji, M., et al. 2019, Monthly Notices of the Royal Astronomical Society, 486, 5335

Collin, S., Kawaguchi, T., Peterson, B. M., & Vestergaard, M. 2006, A&A, 456, 75, doi: 10.1051/0004-6361:20064878

Dalla Bontà, E., Peterson, B. M., Bentz, M. C., et al. 2020, ApJ, 903, 112, doi: 10.3847/1538-4357/abbc1c

Diamond-Stanic, A. M., & Rieke, G. H. 2012, ApJ, 746, 168, doi: 10.1088/0004-637X/746/2/168

Fausnaugh, M. M., Grier, C. J., Bentz, M. C., et al. 2017, The Astrophysical Journal, 840, 97, doi: 10.3847/1538-4357/aa6d52

Grier, C. J., Trump, J. R., Shen, Y., et al. 2017, ApJ, 851, 21, doi: 10.3847/1538-4357/aa98dc

Grier, C. J., Shen, Y., Horne, K., et al. 2019, ApJ, 887, 38, doi: 10.3847/1538-4357/ab4ea5

Homayouni, Y., Trump, J. R., Grier, C. J., et al. 2020, ApJ, 901, 55, doi: 10.3847/1538-4357/ababa9

Horne, K., De Rosa, G., Peterson, B. M., et al. 2021, ApJ, 907, 76, doi: 10.3847/1538-4357/abce60

Kaspi, S., Brandt, W. N., Maoz, D., et al. 2021, ApJ, 915, 129, doi: 10.3847/1538-4357/ac00aa

Kinemuchi, K., Hall, P. B., McGreer, I., et al. 2020, ApJS, 250, 10, doi: 10.3847/1538-4365/aba43f

Kormendy, J., & Ho, L. C. 2013, ARA&A, 51, 511, doi: 10.1146/annurev-astro-082708-101811

Krolik, J. H. 2001, ApJ, 551, 72, doi: 10.1086/320091

Li, Y.-R., Wang, J.-M., Hu, C., Du, P., & Bai, J.-M. 2014, ApJL, 786, L6, doi: 10.1088/2041-8205/786/1/L6

Lira, P., Kaspi, S., Netzer, H., et al. 2018, ApJ, 865, 56, doi: 10.3847/1538-4357/aada45

—. 2020, ApJ, 892, 156, doi: 10.3847/1538-4357/ab6f68

Masoura, V. A., Mountrichas, G., Georgantopoulos, I., & Plionis, M. 2021, A&A, 646, A167, doi: 10.1051/0004-6361/202039238

Nemmen, R. 2021, BCES: Linear regression for data with measurement errors and intrinsic scatter, Astrophysics Source Code Library, record ascl:2110.020. http://ascl.net/2110.020

Onken, C. A., Ferrarese, L., Merritt, D., et al. 2004, ApJ, 615, 645, doi: 10.1086/424655

Peterson, B. M. 1993, PASP, 105, 247, doi: 10.1086/133140

Peterson, B. M., Ferrarese, L., Gilbert, K. M., et al. 2004, ApJ, 613, 682, doi: 10.1086/423269

Shen, Y., Brandt, W. N., Dawson, K. S., et al. 2015, ApJS, 216, 4, doi: 10.1088/0067-0049/216/1/4

Shen, Y., Horne, K., Grier, C. J., et al. 2016, ApJ, 818, 30, doi: 10.3847/0004-637X/818/1/30

Shen, Y., Grier, C. J., Horne, K., et al. 2019, ApJL, 883, L14, doi: 10.3847/2041-8213/ab3e0f

Shirasaki, Y., Akiyama, M., Toba, Y., He, W., & Goto, T. 2020, PASJ, 72, 60, doi: 10.1093/pasj/psaa037

Sun, M., Grier, C. J., & Peterson, B. M. 2018, PyCCF: Python Cross Correlation Function for reverberation mapping studies, Astrophysics Source Code Library, record ascl:1805.032. http://ascl.net/1805.032

Vestergaard, M., & Peterson, B. M. 2006, ApJ, 641, 689, doi: 10.1086/500572

Williams, P. R., Pancoast, A., Treu, T., et al. 2020, ApJ, 902, 74, doi: 10.3847/1538-4357/abbad7

Woo, J.-H., Yoon, Y., Park, S., Park, D., & Kim, S. C. 2015, ApJ, 801, 38, doi: 10.1088/0004-637X/801/1/38

Yu, L.-M., Bian, W.-H., Zhang, X.-G., et al. 2020, ApJ, 901, 133, doi: 10.3847/1538-4357/abb01e

Zu, Y., Kochanek, C. S., Kozłowski, S., & Udalski, A. 2013, ApJ, 765, 106, doi: 10.1088/0004-637X/765/2/106

Zu, Y., Kochanek, C. S., & Peterson, B. M. 2011, ApJ, 735, 80, doi: 10.1088/0004-637X/735/2/80

Zuo, W., Wu, X.-B., Fan, X., et al. 2020, The Astrophysical Journal, 896, 40